PCCP

Gaseous Cyclodextrin-closo-Dodecaborate Complexes XCD·[B12X12]2- (X = α, β, γ; X = F, Cl, Br, I): Electronic Structures and Intramolecular Interactions

Journal:	*Physical Chemistry Chemical Physics*
Manuscript ID	CP-ART-03-2021-001131.R1
Article Type:	Paper
Date Submitted by the Author:	20-Apr-2021
Complete List of Authors:	Jiang, Yanrong; East China Normal University, State Key Laboratory of Precision Spectroscopy Yuan, Qinqin; Pacific Northwest National Laboratory, Physical Sciences Division Cao, Wenjin; Pacific Northwest National Laboratory, Physical Sciences Division Rohdenburg, Markus; Universität Bremen Institut für Angewandte und Physikalische Chemie, Fachbereich 2-Biologie/Chemie Nierstenhöfer, Marc; Bergische Universitat Wuppertal, FK 04 Anorganische Chemie Li, Zhipeng ; East China Normal University, State Key Laboratory of Precision Spectroscopy Yang, Yan; East China Normal University, State Key Laboratory of Precision Spectroscopy Zhong, Cheng; Wuhan University Jenne, Carsten; Bergische Universitat Wuppertal, Fakultät für Mathematik und Naturwissenschaften Warneke, Jonas; Wilhelm-Ostwald-Institut für Physikalische und Theoretische Chemie, Fakultät für Chemie und Mineralogie Sun, Haitao; State Key Laboratory of Precision Spectroscopy, Department of Physics Sun, Zhenrong; East China Normal University, State Key Laboratory of Precision Spectroscopy Wang, Xue-Bin; Pacific Northwest National Laboratory, Physical Sciences Division

SCHOLARONE™
Manuscripts

Gaseous Cyclodextrin-*closo*-Dodecaborate Complexes $\chi CD \cdot [B_{12}X_{12}]^{2-}$ (χ = α, β, γ; X = F, Cl, Br, I): Electronic Structures and Intramolecular Interactions

Yanrong Jiang,[1] Qinqin Yuan,[2] Wenjin Cao,[2] Markus Rohdenburg,[3,4] Marc C. Nierstenhöfer,[5] Zhipeng Li,[1] Yan Yang,[1] Cheng Zhong,[6] Carsten Jenne,[5] Jonas Warneke,[3,7] Haitao Sun,[1,8*] Zhenrong Sun,[1,8*] and Xue-Bin Wang[2*]

[1] *State Key Laboratory of Precision Spectroscopy, School of Physics and Electronic Science, East China Normal University, Shanghai 200241, China*

[2] *Physical Sciences Division, Pacific Northwest National Laboratory, 902 Battelle Boulevard, P.O. Box 999, Richland, Washington 99352, USA*

[3] *Wilhelm-Ostwald-Institut für Physikalische und Theoretische Chemie, Universität Leipzig, 04103 Leipzig, Germany.*

[4] *Institut für Angewandte und Physikalische Chemie, Universität Bremen, Fachbereich 2-Biologie/Chemie, 28359 Bremen, Germany.*

[5] *Fakultät für Mathematik und Naturwissenschaften, Anorganische Chemie, Bergische Universität Wuppertal, Gaußstr. 20, 42119 Wuppertal Germany,*

[6] *College of Chemistry & Molecular Sciences, Wuhan University, Wuhan, Hubei 430072, China*

[7] *Leibniz Institute of Surface Engineering (IOM), Sensoric Surfaces and Functional Interfaces, Permoserstr. 15, D-04318 Leipzig, Germany.*

[8] *Collaborative Innovation Center of Extreme Optics, Shanxi University, Taiyuan, Shanxi 030006, China*

*Corresponding authors: htsun@phy.ecnu.edu.cn (H.-T.S); zrsun@phy.ecnu.edu.cn (Z.-R.S); xuebin.wang@pnnl.gov (X.-B.W.)

Abstract

A fundamental understanding of cyclodextrin-*closo*-dodecaborate inclusion complexes has become of great interest in supramolecular chemistry. Herein, we report a systematic investigation on the electronic structure and intramolecular interactions of perhalogenated *closo*-dodecaborate dianions $B_{12}X_{12}^{2-}$ (X= F, Cl, Br and I) binding to α-, β-, and γ-cyclodextrins (CDs) in the gas phase using combined negative ion photoelectron spectroscopy (NIPES) and density functional theory (DFT) calculations. The vertical detachment energy (VDE) of each complex and electronic stabilization of each dianion due to the CD binding (ΔVDE, relative to the corresponding isolated $B_{12}X_{12}^{2-}$) are determined from the experiments along α-, β-, γ-CD in the form of VDE (ΔVDE): 4.00 (2.10), 4.33 (2.43), 4.30 (2.40) eV in X = F; 4.09 (1.14), 4.64 (1.69), 4.69 (1.74) eV in X = Cl; 4.11 (0.91), 4.58 (1.38), 4.70 (1.50) eV in X = Br; and 3.54 (0.74), 3.88 (1.08), 4.05 (1.25) eV in X = I, respectively. All complexes have significant higher VDEs than the corresponding isolated dodecaborate dianions with the ΔVDE spanning from 0.74 eV at (α, I) to 2.43 eV at (β, F), sensitive to both host CD size and guest substituent X. DFT optimized complex structures exhibit that all $B_{12}X_{12}^{2-}$ prefer binding to the wide openings of CDs with the insertion depth and binding motif strongly dependent on the CD size and halogen X. Dodecaborate anions with heavy halogens, i.e. X = Cl, Br, I, are found outside of α-CD, while $B_{12}F_{12}^{2-}$ is completely wrapped by γ-CD. Partial embedment of $B_{12}X_{12}^{2-}$ into CDs are observed for the other complexes via multi-pronged B-X···H-O/C interlocking patterns. The simulated spectra based on density of states agree well with the experiments and the calculated VDEs well reproduce the experimental trends. Molecular orbital analyses suggest that the spectral features at low binding energies originated from electrons detached from the dodecaborate dianion, while those at higher binding energies derived from electron detachment from CDs. Energy decomposition analyses reveal the electrostatic interaction plays a dominating role in contributing to the host-guest interactions for the X = F series partially due to the formation of O/C-H···X-B hydrogen bonding network, and the dispersion forces gradually become important with the increase of halogen size.

Introduction

The *closo*-dodecaborate dianion $B_{12}H_{12}^{2-}$ and halogenated derivatives $B_{12}X_{12}^{2-}$ (X = H, F-I) belong to the most well-known boron-based molecules with exceptionally high electronic and structural stability.[1-3] These compounds and their derivatives have attracted increasing research interest due to their importance in numerous applications including those in medical diagnosis and cancer treatment,[4-6] in stabilizing reactive cations,[7-12] in catalysis,[13,14] and in designing optoelectronic materials.[15] A fundamental understanding of molecular interactions and noncovalent binding of $B_{12}X_{12}^{2-}$ with various host molecules may contribute to develop efficient delivery reagents into targeted cells (relevant for medical applications including boron-based neutron capture therapy (BNCT) of cancer),[16,17] and have recently gained significant attention as well. Nau and coworkers observed strong affinities of dodecaborate clusters binding to γ-cyclodextrin (CD) in aqueous solution using ^{1}H NMR spectroscopy. The driving force for such strong bindings of the charged guests to CD cavities was attributed to the superchaotropic effect,[18,19] in which hydrophobic binding pockets of CDs preferentially interact with chaotropic dodecaborates in solutions. The intrinsic intermolecular interactions between dianionic halogenated $B_{12}X_{12}^{2-}$ (X = F-I), macropolyhedral boron hydrides and several neutral organic receptors including tetrathiafulvalene (TTF)- and CD-based hosts have been studied in the gas phase using electrospray ionization mass spectrometry.[17,20,21]

Very recently, we reported a joint negative ion photoelectron spectroscopy (NIPES) and computational study on the electronic structures of CDs·$B_{12}X_{12}^{2-}$ (X = H, F) complexes in the gas phase. Strong electronic stabilization effect was observed due to the formation of B-H···H-O dihydrogen bonds in CDs·$B_{12}H_{12}^{2-}$ and B-F···H-O/C traditional hydrogen bonding in CDs·$B_{12}F_{12}^{2-}$.[22] In this work, we present NIPES study of nine CDs·$B_{12}X_{12}^{2-}$ (α-, β-, γ-CD; X = Cl, Br and I) complexes, whose structures are theoretically modeled by inserting $B_{12}X_{12}^{2-}$ into the wide openings of CD cavities. To provide a comprehensive and consistent analysis, the previous experimental results on isolated $B_{12}X_{12}^{2-}$ dianions (X = F-I)[2] and CDs·$B_{12}F_{12}^{2-}$ complexes[22] are also included, but recalculated at the same level of theory used for those CDs·$B_{12}X_{12}^{2-}$ of heavier halogens. The calculated vertical detachment energies (VDEs) and simulated NIPE spectra based on density of states (DOS) of Kohn-Sham orbital energy levels

agree very well with the experiments. Subsequent intermolecular interaction analyses between CDs and $B_{12}X_{12}^{2-}$ are performed based on symmetry-adapted perturbation theory (SAPT) and canonical energy decomposition analysis (EDA) formalisms, unravelling detailed component-specific (i.e. electrostatic, induction, dispersion, and repulsion) contributions. This work thus completes a comprehensive molecular-level investigation about the direct intermolecular interactions of CDs with $B_{12}X_{12}^{2-}$ along the matrix of three different sized CDs and four different perhalogenated dodecaborates without the perturbation of other solvent molecules, providing deep insights into their electronic structures and revealing their molecular properties strongly dependent on the combination of halogen X and CD size.

Experimental Section

The NIPES experiments were carried out using an apparatus consisting of an electrospray ionization source, a cryogenic ion trap and a magnetic bottle time-of-flight photoelectron spectrometer.[23] The CDs·$B_{12}Cl_{12}^{2-}$ and CDs·$B_{12}Br_{12}^{2-}$ complex anions were produced by spraying 0.1 mM mixture solutions prepared by blending the aqueous corresponding sodium salts and CDs solutions with a 3:1 ratio, then diluted 3 times in CH_3OH. Because of the extremely low solubility of the organic $(Et_3NH)_2B_{12}I_{12}$ salt in H_2O, CDs·$B_{12}I_{12}^{2-}$ were produced by spraying 0.1 mM methanolic solution of $(Et_3NH)_2B_{12}I_{12}$ added with aqueous CD solutions in 3:1 ratio. All CDs·$B_{12}X_{12}^{2-}$ dianions generated were guided by two rf-only quadrupoles and a 90° ion bender into the cryogenic ion trap, where they were accumulated and cooled for 20-100ms by collisions with cold buffer gas (20% H_2 balanced in helium) at 20 K, before being pulsed out to the extraction zone of a TOF mass spectrometer. Such a cooling process reduces the influence of hot bands with the appearance of improvement of the spectral energy resolution. For each NIPES experiment, the targeted CDs·$B_{12}X_{12}^{2-}$ complexes were mass selected and maximally decelerated before being photodetached by 157nm (7.866 eV) photons from an F2 excimer laser. The laser was operated at a 20 Hz repetition rate with the ion beam off at alternating laser shots enabling shot-by-shot background subtraction. Photoelectrons were collected at nearly 100% efficiency by the magnetic bottle and analyzed in a 5.2 m long calibrated electron flight tube with 2% energy resolution (i.e., ~20 meV for 1 eV kinetic energy

electrons). The used $[B_{12}X_{12}]^{2-}$ dianions (X = F-I) were prepared according to procedures in the literature.[24-26] For generation of the corresponding sodium salts the triethylammonium salts were reacted with sodium hydroxide followed by the removal of evolving triethylamine at elevated temperature in vacuo.

Computational Details

Due to the complexity of interactions between neutral CD hosts and anionic $B_{12}X_{12}^{2-}$ guests and expected plethora of conformers, an optimization strategy combining a global semi-empirical quantum mechanical method and density functional theory was adopted to ensure the most stable structures being obtained. Initially, more than one hundred of molecular configurations were generated using Molclus,[27] followed by semi-empirical optimization at the PM6-D3H4[28,29] level using the MOPAC program.[30] Thirty lowest-lying structures were thus obtained according to their energy levels and re-optimized using more accurate DFT method at the M06-2X[31]-D3/def2-SVP[32,33] level with Grimme's popular D3 correction employed for the reliable treatment of dispersion interactions.[34] The subsequent single point (SP) energies at the level of M06-2X-D3/ma-TZVP[32,33,35,36] were carried out to ensure the lowest-lying structures. Those lowest-lying structures were re-optimized at the M06-2X-D3/TZVP[37-39] level. The quasi-relativistic energy-adjusted ab initio Stuttgart pseudopotentials (ECP46MWB) included in TZVP basis and the fully relativistic small-core Stuttgart pseudopotentials (ECP28oldMDF) included in ma-TZVP basis were employed for atomic iodine (I), respectively. The theoretical VDEs were computed as the SP M06-2X-D3/ma-TZVP energy differences between $CDs{\cdot}B_{12}X_{12}^{-}$ and corresponding $CDs{\cdot}B_{12}X_{12}^{2-}$, both at the optimized dianion geometries. The M06-2X functional has been shown as one of the top performers for main group thermochemistry, kinetics and non-covalent interactions,[40] and is thus employed here. The suitability of the current theoretical method is confirmed by comparing the experimental and M06-2X calculated VDEs with an acceptable mean average deviation of 0.13 eV. Note that the combination of basis sets employed herein (TZVP for geometry optimization and ma-TZVP for SP calculation) is different from that used in our previous work of $CDs{\cdot}B_{12}X_{12}^{2-}$ (X = H, F) (6-311G(d,p) for geometry optimization and 6-311+G(d,p) for SP

calculation)[22] with the current one showing overall better accuracy (see Table S1). The intermolecular binding energies (BEs) between $B_{12}X_{12}^{2-}$ and CDs were calculated as the energy differences between the complexes and unrelaxed CDs and $B_{12}X_{12}^{2-}$, based on the optimized CDs·$B_{12}X_{12}^{2-}$ geometries including the basis set superposition error (BSSE) correction using the Boys and Bernardi counterpoise method.[41] The DOS of Kohn-Sham orbital energy levels of CDs·$B_{12}X_{12}^{2-}$ complexes were used to simulate theoretical photoelectron spectra. Element-based partial DOS simulations were calculated by Hirshfeld partition method, where Hirshfeld weighting of an atom $\omega_{atom}(r)$ was used for decomposing orbital into fragment composition based on the atomic densities of all atoms in specific fragment, the composition of fragment A in orbital i is the sum of compositions of the atoms ($\int \varphi_i^2(r)\omega_{atom}(r)dr \times 100\%$) belong to the fragment.[42,43] The symmetry-adapted perturbation theory (SAPT)[44] at the exchange-scaled SAPT0 (sSAPT0)[45-47]/jun-cc-pVDZ(-pp)[48,49] level is further applied to decompose the BE into four physically meaningful components, *i.e.*, electrostatic, induction, dispersion and exchange-repulsion contribution using PSI4 code.[50] Complementarily, the canonical energy decomposition analysis (EDA) using a Morokuma-Ziegler-type energy decomposition scheme was performed at the B3LYP[51]-D3(BJ)/TZ2P level using ADF software.[52,53] The definition of interaction energy in EDA is slightly different from that of SAPT, and consists of three physically meaningful terms, including classical electrostatic, orbital interaction and Pauli repulsion. Note that empirical dispersion was included into the interaction energy as introduced by Grimme and co-workers.[34,54] The independent gradient model (IGM), widely utilized in the analyses of intra-/intermolecular weak interactions in biology and chemistry,[55,56] was employed to intuitively display the non-covalent interaction in the molecular complexes investigated here. The highest occupied molecular orbitals (HOMO), electrostatic potential maps, and restrained electrostatic potential (RESP) charges were generated by the Multiwfn code[43] and the corresponding isosurfaces were rendered by the VMD program.[57] All DFT M06-2X calculations and natural population analysis (NPA) charges were carried out using the Gaussian 16 software.[58] The topology of the electron density was examined in the frame of a Quantum Theory of Atoms In Molecules (QTAIM)[59] analysis with the Multiwfn program.[43]

RESULTS AND DISCUSSION

NIPE spectra of CDs·$B_{12}X_{12}^{2-}$

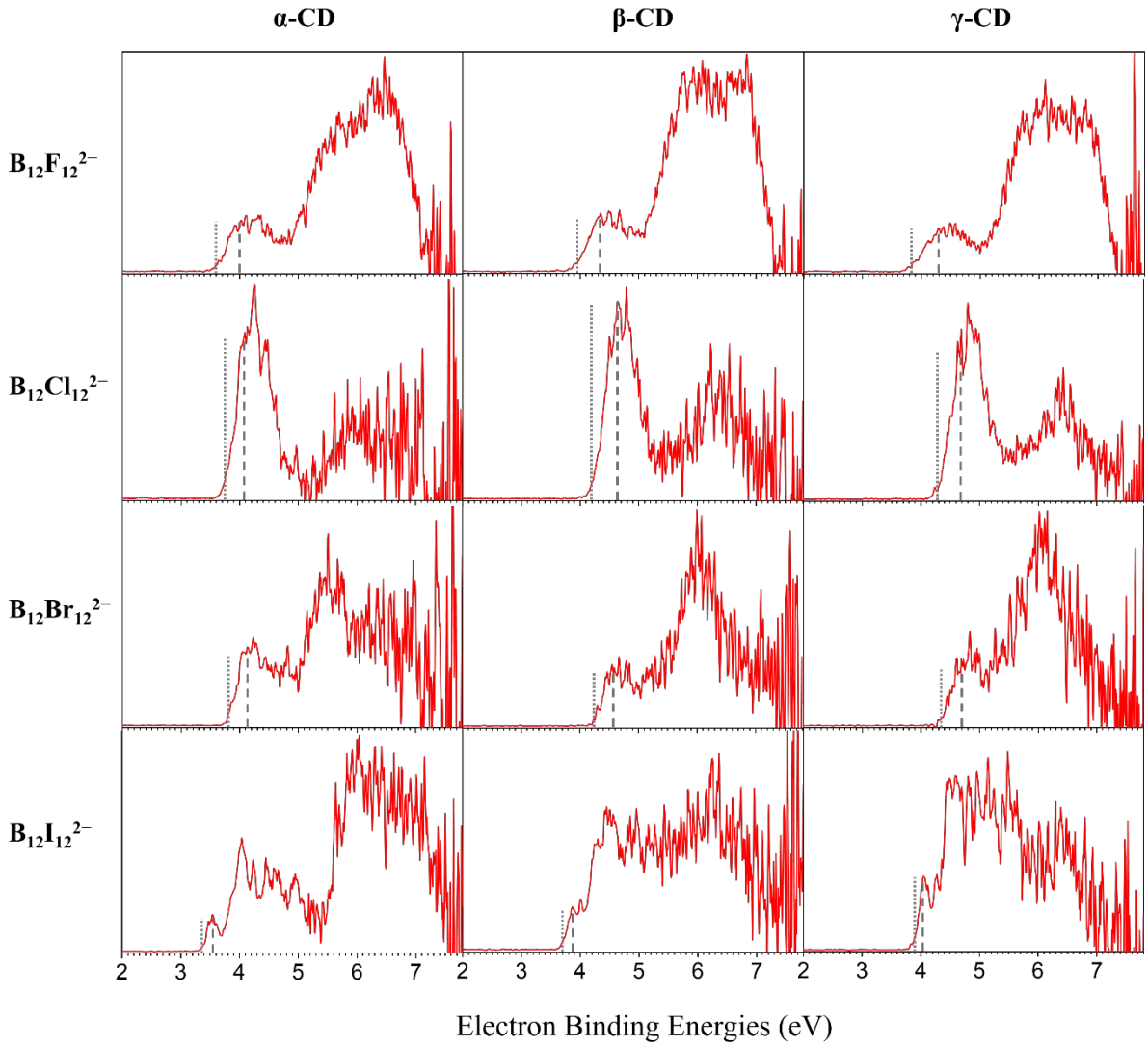

Fig. 1 The 20K NIPE spectra of χCD·$B_{12}X_{12}^{2-}$ (χ = α-, β-, γ-; X = F, Cl, Br, and I) measured with 157 nm photons. The measured spectra for the X=F series are adapted from reference [22]. The gray dotted and dashed lines designate the spectral EBE positions from which the ADEs and VDEs are determined, respectively.

Fig. 1 shows the 20 K 157 nm NIPE spectra for a complete series of χCD·$B_{12}X_{12}^{2-}$ (χ = α-, β-, γ-; X = F, Cl, Br, and I). The electron binding energies (EBEs) of CDs·$B_{12}X_{12}^{2-}$ complexes are significantly larger than the corresponding isolated $B_{12}X_{12}^{2-}$, indicating strong electronic stabilization of $B_{12}X_{12}^{2-}$ upon complex formation with CDs, but to a varying degree.

The experimental adiabatic detachment energies (ADEs) were estimated from the spectral onset threshold, while the vertical detachment energies (VDEs) were measured from the spectral peak of the first resolved band, as indicated by the gray dotted and dashed lines, respectively in Fig. 1. As listed in Table 1, the ADEs are consistently smaller than the corresponding VDEs, by 0.4, 0.4, 0.3, and 0.2 eV on average for X = F, Cl, Br, and I, respectively. For a given X, the VDE increases from α- to β- and γ-CD; while for given CD, the VDE noticeably increases from X = F to X = Cl, Br, followed by appreciable decrease at X = I (Fig. 2a), similar to the VDE trend of isolated $B_{12}X_{12}^{2-}$. The largest binding stabilization is observed for the fluorine series for all CDs. The measured VDEs of β-CD·$B_{12}X_{12}^{2-}$ and γ-CD·$B_{12}X_{12}^{2-}$ are close to each other and both larger than those of α-CD·$B_{12}X_{12}^{2-}$ by 0.47 eV on average. The highest VDE measured among all 12 complexes amounts to 4.70 eV for γ-CD·$B_{12}Br_{12}^{2-}$, a value that is exceptionally high in the context of gaseous multiply charged anions but still 1 eV lower than the VDE of the record holder — isolated $[B_{12}(CN)_{12}]^{2-}$ dianion.[60] The VDE increases of CDs·$B_{12}X_{12}^{2-}$ with respect to the isolated dodecaborate anions, *i.e.*, ΔVDEs, are largest for X = F, and gradually decrease with the increase in halide size (Fig. 2c).

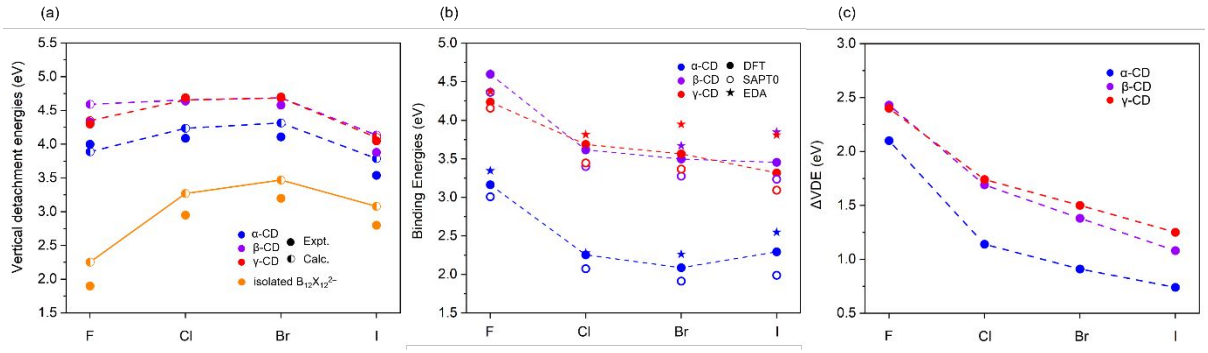

Fig. 2 (a) Experimental (filled circles) and calculated (semi-solid circles) VDEs of isolated $B_{12}X_{12}^{2-}$ dodecdaborate anions and CDs·$B_{12}X_{12}^{2-}$ complexes (X = F — I); (b) Calculated binding energies of CDs·$B_{12}X_{12}^{2-}$ at the levels of M06-2X-D3/ma-TZVP (solid circles), sSAPT0/jun-cc-pVDZ(-pp) (open circles), and B3LYP-D3(BJ)/TZ2P (EDA) (stars); (c) Experimental ΔVDEs determined as VDE differences between CDs·$B_{12}X_{12}^{2-}$ and the corresponding isolated $B_{12}X_{12}^{2-}$.

Table 1 (a) Experimental adiabatic / vertical detachment energies (ADEs / VDEs), and calculated VDEs of CDs·$B_{12}X_{12}^{2-}$ (X = F – I); (b) Binding energies (BEs) of CDs·$B_{12}X_{12}^{2-}$ calculated at the M06-2X-D3/ma-TZVP, sSAPT0/jun-cc-pVDZ(-pp), and B3LYP-D3(BJ)/TZ2P (EDA) levels of theory. All energies are in eV.

(a)

	$B_{12}F_{12}^{2-}$		$B_{12}Cl_{12}^{2-}$		$B_{12}Br_{12}^{2-}$		$B_{12}I_{12}^{2-}$	
	Expt.[a]	Calc.	Expt.[a]	Calc.	Expt.[a]	Calc.	Expt.[a]	Calc.
	(1.70) 1.90[b]	2.25	(2.77) 2.95[b]	3.27	(2.98) 3.20[b]	3.47	(2.75) 2.80[b]	3.08
α-CD	(3.60) 4.00[c]	3.89	(3.75) 4.09	4.24	(3.80) 4.11	4.32	(3.35) 3.54	3.79
β-CD	(3.95) 4.33[c]	4.59	(4.20) 4.64	4.66	(4.25) 4.58	4.69	(3.70) 3.88	4.14
γ-CD	(3.85) 4.30[c]	4.35	(4.30) 4.69	4.66	(4.35) 4.70	4.69	(3.90) 4.05	4.10

[a] Experimental (ADE) VDE with 0.1 eV uncertainty for all complexes; [b] from reference 2; [c] from reference [22].

(b)

BE	$B_{12}F_{12}^{2-}$			$B_{12}Cl_{12}^{2-}$			$B_{12}Br_{12}^{2-}$			$B_{12}I_{12}^{2-}$		
	M062X	SAPT0	EDA	M062X	SAPT0	EDA	M062X	SAPT0	EDA	M062X	SAPT0	EDA
α-CD	3.16	3.01	3.35	2.25	2.08	2.28	2.09	1.91	2.26	2.29	1.99	2.55
β-CD	4.60	4.37	4.60	3.61	3.40	3.62	3.50	3.28	3.67	3.46	3.24	3.85
γ-CD	4.24	4.16	4.37	3.69	3.45	3.82	3.56	3.37	3.95	3.32	3.09	3.81

Low-lying structures and energetics of CDs·$B_{12}X_{12}^{2-}$ complexes

Table 2 Calculated penetrating distance (P index) between CDs and $B_{12}X_{12}^{2-}$ (X = F – I)[a].

P index /Å	$B_{12}F_{12}^{2-}$	$B_{12}Cl_{12}^{2-}$	$B_{12}Br_{12}^{2-}$	$B_{12}I_{12}^{2-}$
α-CD	-1.96	-3.26	-3.79	-4.18
β-CD	-0.02	-1.88	-2.23	-3.06
γ-CD	2.34	-0.75	-1.15	-1.76

[a]see Fig. S1 for P index definition.

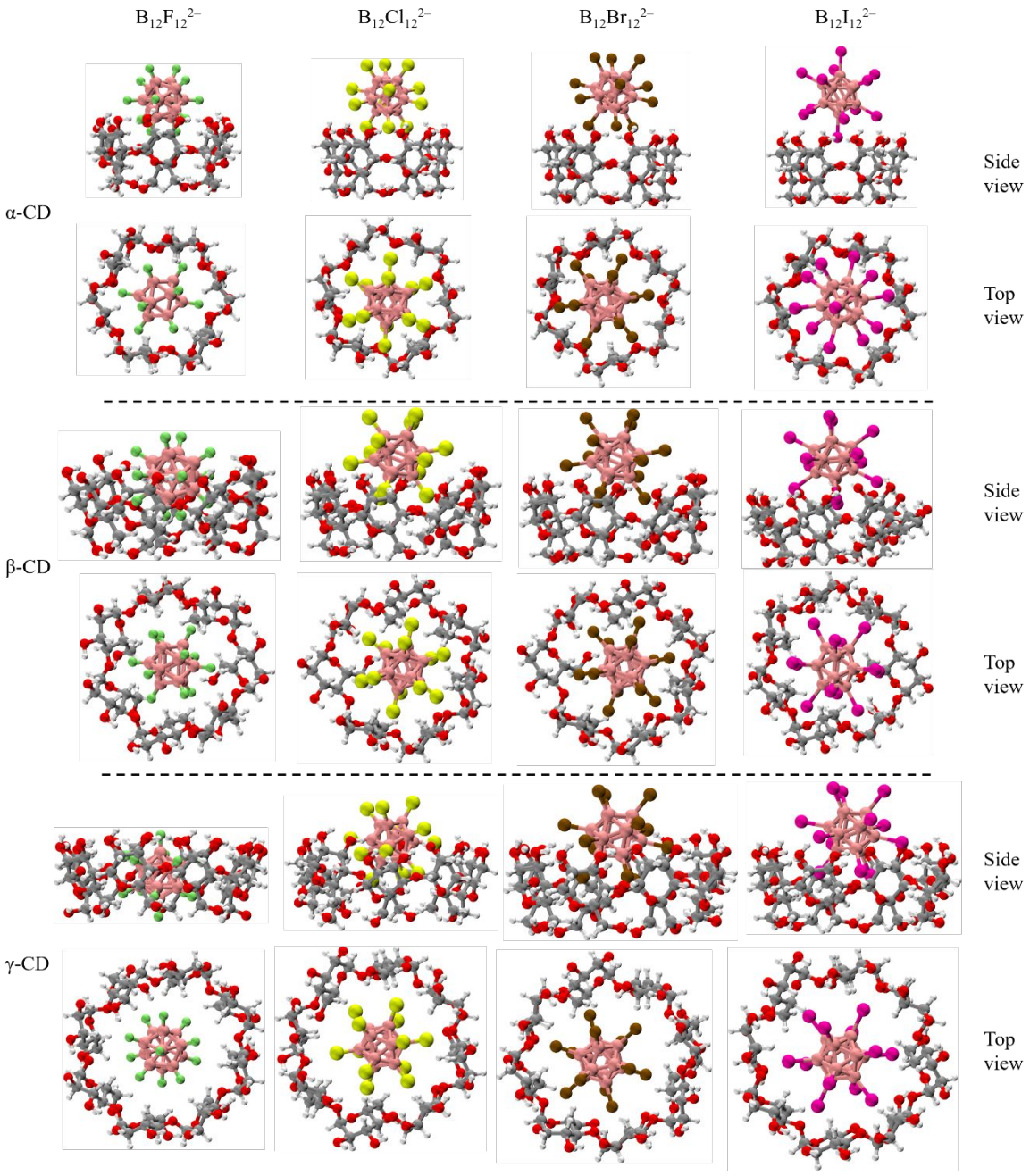

Fig. 3 M062X-D3/TZVP optimized structures of CDs·$B_{12}X_{12}^{2-}$ (X = F – I) with side and top views. Pink, green, yellow, brown, magenta, silver, red, and white balls denote boron (B), fluorine (F), chlorine (Cl), bromine (Br), iodine (I), carbon (C), oxygen (O), hydrogen (H) atoms, respectively.

The complexity of the systems studied here demands three questions to be first answered before conducting full theoretical investigations: 1) which opening of CDs that $B_{12}X_{12}^{2-}$ prefers to bind to; 2) what kind of basis set is sufficient to depict the complex structures; and 3) which

DFT functional performs well with respect to the experimental results? Our M06-2X-D3/ma-TZVP calculations for β-CD·$B_{12}F_{12}^{2-}$ show that the dodecaborate anion prefers interacting with the wide opening of β-CD (4.9 kcal/mol more stable, Table S2). Noticeable conformation changes were seen by increasing the basis set from def2-SVP to TZVP for M06-2X-D3 optimizations (Fig. S2). Further increasing basis set from TZVP to def2TZVPP, however, results in marginal structural variations (Fig. S3). Optimized geometries obtained using three different functionals, i.e., PBE0+GD3BJ, B3LYP+GD3BJ, M06-2X-D3, all with TZVP basis set lead to very similar structures (Fig. S4). The structural differences have minor effect on the calculated VDEs done with a particular functional (e.g. M06-2X-D3/ma-TZVP level (Table S3)). However, the VDE calculated with the different methods on the same geometry shows strong deviations – both B3LYP and PBE0 underestimate the VDEs compared to the experimental values, while M06-2X gives relatively the best results (Table S4, S5). Therefore, in the following sections, we present computational results based on M06-2X-D3/TZVP optimization and SP M062X-D3/ma-TZVP energy calculations unless otherwise noticed.

Fig. 3 shows the optimized structures of CDs·$B_{12}X_{12}^{2-}$ (X = F-I). Apparently, α-, β- and γ-CD hosts tend to have different binding affinities to halogenated dodecaborate anion guests. For α-CD, $B_{12}X_{12}^{2-}$ (X = Cl, Br, I) cannot penetrate into the α-CD ring but $B_{12}F_{12}^{2-}$ is partly embedded. Only for the combination of γ-CD and $B_{12}F_{12}^{2-}$, the dianion guest is maximally penetrated into the host molecule and appears fully "wrapped", while even for γ-CD all larger $B_{12}X_{12}^{2-}$ are only partly embedded to varying degrees according to their size. To quantify the degree of penetration of $B_{12}X_{12}^{2-}$ into the CD opening, we define the penetrating distance (P index), which was measured as the distance between the best-fit plane (i.e. least-squares plane defined in Fig. S1) of 2,3-oxygens of the wide opening of CDs and the mass center of $B_{12}X_{12}^{2-}$ dianions that have penetrated through the defined plane. As shown in Table 2, the P index values are ranged from -4.18 to 2.34 Å. The P values decrease as the size of halogen atom increases from α- to γ-CD series. The negative P values indicate that these larger dodecaborate anions suspend above the CDs wide opening at low degree of penetrating. Interestingly, except for α-CD·$B_{12}I_{12}^{2-}$ and γ-CD·$B_{12}F_{12}^{2-}$, in which B-X bond is approximatively perpendicular to the CD opening, all other complexes exhibit $B_{12}X_{12}^{2-}$ being rotated with respect to CDs in a fashion that enables multi-pronged interlocking binding motifs that was previously proposed

in binding with $C_6F_6H_6$.[61] Specifically, for α-CD·$B_{12}F_{12}^{2-}$, β-CD·$B_{12}F_{12}^{2-}$, and β-CD·$B_{12}I_{12}^{2-}$, four prongs with two deeply embedded halogen atoms were placed into the cavity; while for the remaining complexes, three-point interlocking binding motifs driven by the host-guest fields are formed. As expected, the largest penetrating depth is observed for the γ-CD·$B_{12}F_{12}^{2-}$ complex, where the $B_{12}F_{12}^{2-}$ guest is completely wrapped inside the γ-CD cage with only the top and bottom fluorine atoms pointing to the outside.

The BEs between CD and $B_{12}X_{12}^{2-}$ complexes were calculated using M06-2X-D3/ma-TZVP, sSAPT0/jun-cc-pVDZ (jun-cc-pVDZ-pp for I atom) and EDA scheme (Table 1b), all showing similar trends (Fig. 2b). The fluorine series possesses higher BEs with respect to other halogen series, particularly, the β-CD·$B_{12}F_{12}^{2-}$ complex has the largest BE (4.60 eV at M06-2X/ma-TZVP). The smallest BE of 2.09 eV is observed for α-CD·$B_{12}Br_{12}^{2-}$, correlated to the larger negative penetrating index of -3.79 Å. By tuning the halogen series from F to I, the calculated BEs decrease by 0.87 ~ 1.08 eV for the α-CD series, by 0.98 ~ 1.14 eV for the β-CD series and by 0.54 ~ 0.92 eV for the γ-CD series. Alternatively, the BEs increase by 1.02 ~ 1.48 eV by replacing the small α-CD with wider β-CD/γ-CD, confirming a more significant stabilization effect of β-CD/γ-CD. The differences of experimental VDEs between CDs·$B_{12}X_{12}^{2-}$ complexes and isolated $B_{12}X_{12}^{2-}$ (X = F, Cl, Br and I), i.e., ΔVDEs show similar trends as the BEs among different CDs ─ both values for β-CD/γ-CD being substantially larger than those for α-CD. However, ΔVDE exhibits a monotonic decrease along the halogen series for all CDs (Fig. 2c), different from the corresponding curves for BEs, which display a slight increase from Br to I for the α-CD series and plateaus from Cl to I for β-CD/γ-CD.

It should be noted that for complexes with singly charged ions incorporated in a host, the experimental ΔVDEs often match reasonably well with the BEs.[22,62] Here, the absolute ΔVDE values of the dianionic complexes (Table S6) are significantly smaller than the calculated BEs. This is expected because there is still appreciable interaction between CDs and the singly charged $[B_{12}X_{12}]^{\bullet-}$ species after photodetachment. The detailed discussions on the connection and difference between BE and ΔVDE are given in our previous publications.[22,62] In addition, the second lowest-lying structures for α-CD·$B_{12}X_{12}^{2-}$ (X = F, Cl, Br, and I) were calculated to be 1.71 ~ 2.91 kcal/mol higher in energy, and their VDEs were found to be very close to the

most stable structures (Table S7). These results indicate marginal contributions of these low-lying isomers to the experimental spectra which were taken under low temperature conditions.

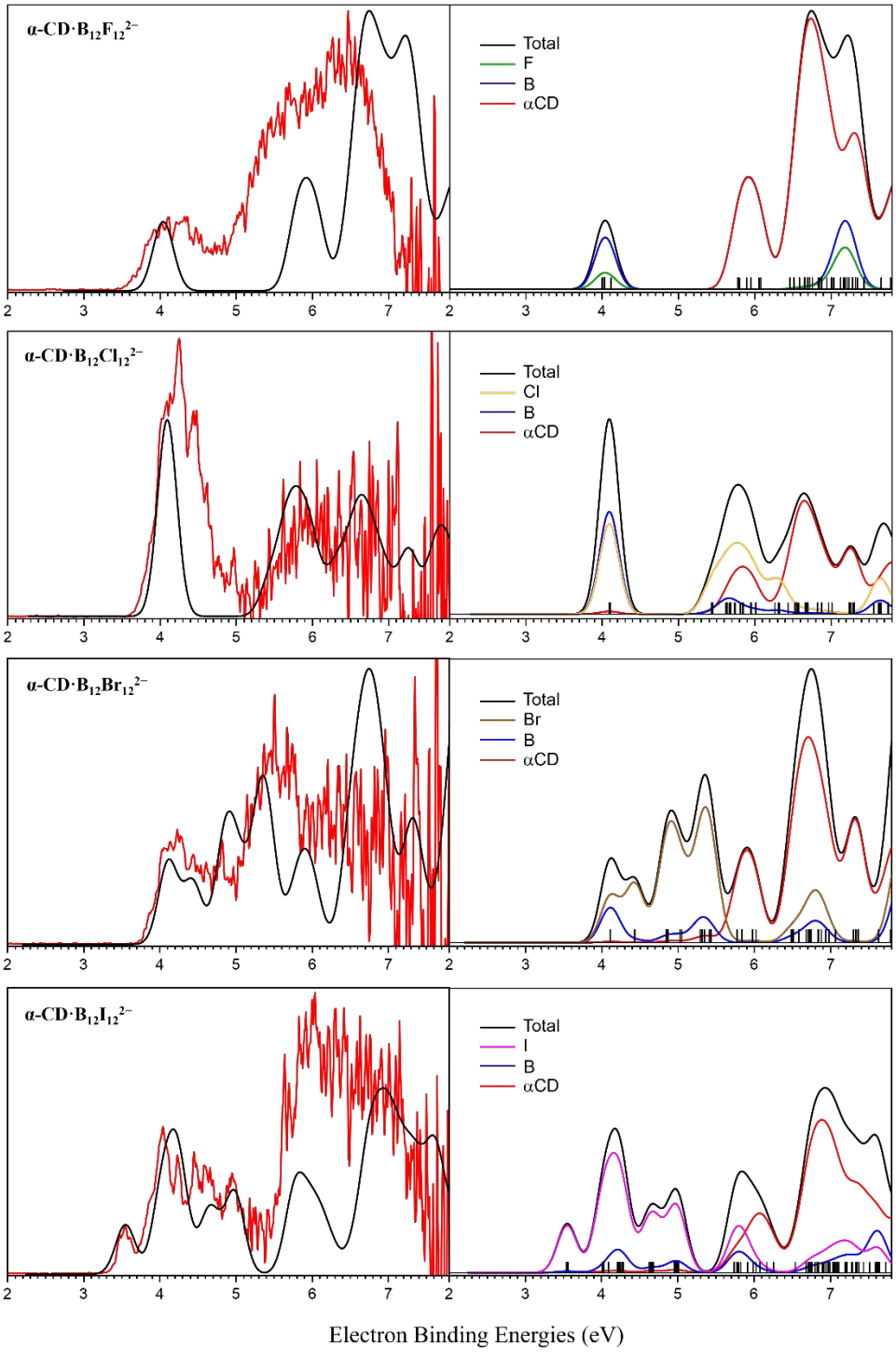

Fig. 4 (Left) Measured (red) and simulated total DOS (black) NIPE spectra of α-CD·$B_{12}X_{12}^{2-}$ (X = F, Cl, Br and I). (Right) Simulated stick spectrum for each complex with the HOMO being shifted to match the experimental VDE. The total DOS and partial DOS (assigned according to the dominant component in specific occupied MOs) spectra were first obtained by

convoluting each stick with a linewidth of 0.30 eV (full width at half maximum) and unit area. Due to the existence of repulsive coulomb barrier (RCB) in photodetaching these dianionic complexes,[63-65] all simulated bands beyond 6 eV are severely suppressed or completely cut off in the experiments. For X = Br and I, partial DOS curves indicate dominant spectral bands below 6 eV coming from halides, therefore no intensity adjustment is applied for these two cases in the simulated DOS. However, for X = F, Cl, different elements are involved in bands in EBE = 0-6 eV. Considering different ionization cross sections for different elements, the simulated spectral intensity was manually adjusted for overall better match with the experimental intensities. For X = F, the intensity due to CD oxygen is scaled up by 1.5 relative to B and F; while for X = Cl, the intensity due to Cl DOS is scaled up by 4.5 relative to B and O. The DOS of β-CD and γ-CD series based on the same treatment are provided in Fig. S5.

Molecular orbital analyses and spectral simulations

The positions of the bands in photoelectron spectra generally reflect the energy differences between various electronic states of the final species after ionization relative to the initial electronic ground state before ionization.[62,66] Under the Koopmans' theorem,[67] the negative eigenvalue of the highest occupied molecular orbital (HOMO) obtained from exact Kohn-Sham DFT should be a good approximation to the experimental VDE, and the spectral bands at high EBE correspond to remove electrons from successive deeper occupied MOs if fully ignoring the orbital relaxation effects. Therefore, we generated the total density of states (DOS) curves to have direct comparison with the experimental spectra, as shown in Fig. 4 and Fig. S5. Overall, the simulated DOS spectra show good agreement with the measured spectra for all CDs·$B_{12}X_{12}^{2-}$ (X = F - I) complexes studied here.

The corresponding contribution of each fragment to the HOMOs of CDs·$B_{12}X_{12}^{2-}$ complexes were calculated as shown in Fig. S7 and listed in Table S8. For a given X, the HOMO composition of each CD·$B_{12}X_{12}^{2-}$ complex is nearly independent of the CD type, and in fact almost the same as the isolated $B_{12}X_{12}^{2-}$. Along the halogen series HOMO composition varies significantly with X: the contribution from B atoms gradually decrease (75%, 53%, 43%, and 3%) and the contribution from halogen shell increases accordingly (24%, 46%, 56%, and 96%) for X = F, Cl, Br, and I, respectively. Although the host CD contributes marginally to the HOMOs of each complex, it destroys the highly icosahedral (I_h) symmetry of $B_{12}X_{12}^{2-}$, resulting in splitting up the original degenerate orbitals (HOMO levels for CDs·$B_{12}X_{12}^{2-}$ are pseudo-degenerate within ~ 0.14 eV, see Fig. 4 and Fig. S5). Additionally, MO analysis clearly

reveals that high-lying MOs are mainly composed of elements boron and halogens, while the oxygens from CDs largely contribute to the deeper MOs, corresponding to the high EBE spectral bands. It is also clear that along the halogen series from F to I, the halogen shells play an increasingly dominant role in contributing to the low EBE bands. Based on the above MO composition analyses, element-based partial DOS spectra are generated (Fig. 4, right), illustrating how each element contributes to the observed spectra. It is evident that progressively more structured spectral features are resolved in the low EBE region from X = Cl to Br and I, which originates from the fact that these low EBE bands are dominated by contributions from Br and I elements, both with large spin-orbit coupling splittings.[68,69] Furthermore, as shown in Fig. S6, the anisotropic characters of occupied molecular orbitals and particularly the fact that halides far away from CDs contribute to low EBE bands and the ones close to CD correspond to high EBE features are the reason for observing more structural halide-dominant bands in low EBE region.

Both natural population analysis (NPA) and restrained electrostatic potential (RESP) confirm that the general development of partial charges along the halogen series in $B_{12}X_{12}^{2-}$ is qualitatively the same in the host-guest complex (Fig. S9) as found for the free dodecaborate dianions,[2] *i.e.*, along the halogen series from F to I, the halogen shell becomes more positive and the inner boron region becomes more negative, with the sign of charge for boron core and halogen shell switched from X = Br to X =I. The combination of HOMO spatial location and charge distribution suggest the most loosely bound electrons being detached for the complexes is progressively shifted from the boron core to halogen shell from F to I, in a similar fashion as for isolated $B_{12}X_{12}^{2-}$.

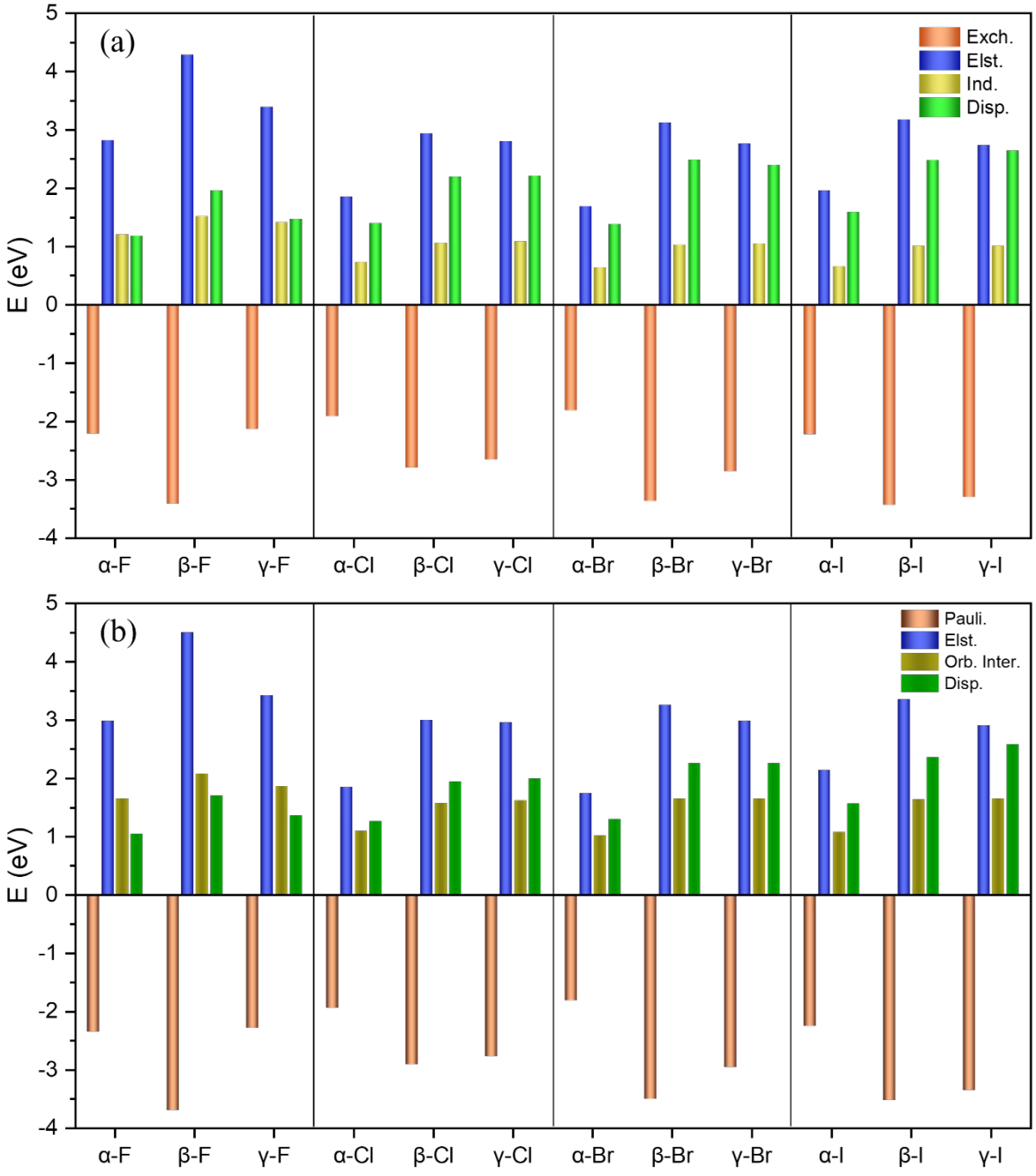

Fig. 5 Components of two different decomposition analysis for CDs·$B_{12}X_{12}^{2-}$ dianions (X = F-I) (a) exchange, electrostatic, induction and dispersion terms from SAPT analysis at the sSAPT0/jun-cc-pVDZ-(pp) level; and (b) Pauli repulsive, electrostatic, orbital interaction, and dispersion derived from EDA (B3LYP-D3(BJ)/TZ2P) analysis.

Analysis of the nature of intermolecular interactions between CDs and $B_{12}X_{12}^{2-}$

The interaction between the CDs and $B_{12}X_{12}^{2-}$ anions was further investigated using two different methods (i) symmetry-adapted perturbation theory (SAPT)[44,70] at the sSAPT0 level,

and (ii) the canonical energy decomposition analysis (EDA).[52,53] Both analyses decompose the total interaction energies into four physically meaningful components. In both cases the electrostatic and the dispersion (although using different approaches) are calculated. Destabilizing exchange interactions are also considered in both methods (SAPT: exchange term, EDA: Pauli Repulsion). The fourth component, the orbital interaction energy provided by the EDA, may be considered qualitatively comparable to the SAPT induction term and the destabilizing Pauli repulsion from the EDA may be compared with the exchange term provided by the SAPT analysis. Fig. 5 compares the three attractive components electrostatic, induction/orbital interaction and dispersion interactions, respectively (also listed in Table S9). The trend for the total binding energies calculated with both methods agree well with the DFT results at the M06-2X-D3/ma-TZVP level (see Fig. 2b). As shown in Fig. 5, the electrostatic interaction E_{elst} is the most attractive force. Interestingly, compared to α-CD·$B_{12}X_{12}^{2-}$ and γ-CD·$B_{12}X_{12}^{2-}$, the series of β-CD·$B_{12}X_{12}^{2-}$ always possess the largest E_{elst} values. This is mainly attributed to the wide opening of β-CD possessing the optimal ring diameter, and such size matching principle leads to more contact opportunities with the halogen atoms of dodecaborate dianions and stronger electrostatic interaction. Meanwhile, the largest BE of β-CD·$B_{12}F_{12}^{2-}$ complex derives from the significant contribution of electrostatics due to the formation of magnificent hydrogen bonding networks. More C-H···X-B and O-H···X-B acting sites between F atoms and secondary hydroxyl groups of β-CD are assembled as intuitively revealed by independent gradient model (IGM) (Fig. S8). To further explore the binding motifs in the host-guest systems, the numbers of two types of hydrogen bond, (C-H···X-B) and (O-H···X-B), in CDs·$B_{12}X_{12}^{2-}$, were counted (shown in Table S10). The criteria to define a hydrogen bond herein is: (i) within a cutoff distance of 3.9 Å between the donor (C/O in CDs) and acceptor (X in $B_{12}X_{12}^{2-}$) and (ii) the bond angle of (D-H···A) larger than 140°. Thirteen C-H···F-B and five O-H···F-B hydrogen bonds of β-CD·$B_{12}F_{12}^{2-}$ are found that are more than that of γ-CD·$B_{12}F_{12}^{2-}$. A QTAIM analysis of the topology of the electron density revealed 16 (α-CD), 40 (β-CD) and 35 (γ -CD) bond paths with a bond critical point between the respective CD and $[B_{12}F_{12}]^{2-}$, which is qualitatively in line with the mentioned explanation. Notably, the dispersion contribution becomes gradually important from F to I, particularly for γ-CD·$B_{12}I_{12}^{2-}$ complex. This can be attributed to their increasing polarizabilities.[2] Last, for β-CD·$B_{12}X_{12}^{2-}$

complexes, the significant reduction of BEs from fluorine to other halogen series is attributed to the greatly decreased electrostatic interaction. Meanwhile, the significantly increased BEs from α-CD to β-CD/γ-CD mainly benefits from the simultaneous increased electrostatic, induction, and dispersion interactions.

5. CONCLUSION AND OUTLOOK

In this work, electronic stability, and non-covalent interactions between three differently sized CD hosts and four different perhalogenated dodecaborate guests $B_{12}X_{12}^{2-}$ (X= F, Cl, Br, I) have been systematically studied employing NIPES and DFT calculations. Our results clearly indicate remarkable size- and molecular specific interactions, *viz*, β-/γ-CDs have significantly stronger affinity than α-CD when binding to each $B_{12}X_{12}^{2-}$, and $B_{12}F_{12}^{2-}$ is preferred over other larger halogenated dodecaborates when binding to each CD. DFT optimized low-lying structures confirm the observed staircase of interactions. Energy decomposition analyses of the host-guest interactions reveal the electrostatic attraction plays a dominant role, driven by the formation of extensive O/C-H···X-B hydrogen bonding network in these complexes. Element-based partial DOS simulations enable distinguishing contributions of $B_{12}X_{12}^{2-}$ and CDs that are responsible for the low and high EBE parts of spectra, respectively. Taken together, this work represents a comprehensive experimental and theoretical study on the electronic and geometric structures over the whole series of CDs·$B_{12}X_{12}^{2-}$ complexes at the fundamental molecular level, and provides insightful perspectives on understanding the intrinsic nature of intermolecular interactions in CDs·$B_{12}X_{12}^{2-}$ host-guest molecular systems that have been widely applied in biomedicinal treatments, separation sciences, and supramolecular chemistry.

Author contributions: H.S., Z.R.S., and X.B.W. designed research; Y.J., Q.Y.; W.C., M.R., Z.L., Y.Y., C.Z., J.W., H.S. conducted research; M.C.N., C.J. contributed new reagents; Y.J., J.W., H.S., M.R., Z.R.S. and X.B.W analyzed data; Y.J., H.S., Z.R.S., J.W. and X.B.W. wrote the paper. All authors contributed to discussions.

Conflicts of interest

There are no conflicts to declare.

ACKNOWLEDGEMENTS

The NIPES work was supported by U.S. Department of Energy (DOE), Office of Science, Office of Basic Energy Sciences, Division of Chemical Sciences, Geosciences, and Biosciences, and performed using EMSL, a national scientific user facility sponsored by DOE's Office of Biological and Environmental Research and located at Pacific Northwest National Laboratory, which is operated by Battelle Memorial Institute for the DOE. The theoretical calculations were supported by National Natural Science Foundation of China (Nos. 12034008, 11727810 and 51873160), Projects from Shanghai Science and Technology Commission (No. 19JC1412200), and the Program of Introducing Talents of Discipline to Universities 111 project (B12024). We acknowledge the ECNU Multifunctional Platform for Innovation (001) and HPC Research Computing Team for providing computational and storage resources. JW is grateful to the Volkswagen foundation for a Freigeist fellowship. MCN is grateful for a Kekulé Fellowship from the Fonds der Chemischen Industrie.

REFERENCES

1 E. Aprà, J. Warneke, S. S. Xantheas and X.-B. Wang, *J. Chem. Phys.*, 2019, **150**, 164306.
2 J. Warneke, G.-L. Hou, E. Aprà, C. Jenne, Z. Yang, Z. Qin, K. Kowalski, X.-B. Wang and S. S. Xantheas, *J. Am. Chem. Soc.*, 2017, **139**, 14749-14756.
3 R. T. Boeré, J. Derendorf, C. Jenne, S. Kacprzak, M. Keßler, R. Riebau, S. Riedel, T. L. Roemmele, M. Rühle, H. Scherer, T. Vent-Schmidt, J. Warneke and S. Weber, *Chem. Eur. J.*, 2014, **20**, 4447-4459.
4 A. H. Soloway, W. Tjarks, B. A. Barnum, F.-G. Rong, R. F. Barth, I. M. Codogni and J. G. Wilson, *Chem. Rev.*, 1998, **98**, 1515-1562.
5 W. H. Sweet, *N. Engl. J. Med.*, 1951, **245**, 875-878.
6 M. F. Hawthorne and A. Maderna, *Chem. Rev.*, 1999, **99**, 3421-3434.
7 C. Bolli, J. Derendorf, M. Keßler, C. Knapp, H. Scherer, C. Schulz and J. Warneke, *ACS Symp. Ser.*, 2010, **49**, 3536-3538.
8 A. Schäfer, M. Reißmann, S. Jung, A. Schäfer, W. Saak, E. Brendler and T. Müller, *Organometallics*, 2013, **32**, 4713-4722.
9 J. Derendorf, C. Jenne and M. Keßler, *Angew. Chem., Int. Ed.*, 2017, **56**, 8281-8284.
10 C. Jenne, M. C. Nierstenhöfer and V. van Lessen, *Chem. Eur. J.*, 2021, **27**, 3288-3291.
11 I. M. Riddlestone, A. Kraft, J. Schaefer and I. Krossing, *Angew. Chem., Int. Ed.*, 2018, **57**, 13982-14024.

12 C. Knapp, Weakly Coordinating Anions: Halogenated Borates and Dodecaborates, in *Comprehensive Inorganic Chemistry II (Second Edition)*, Elsevier, Amsterdam, 2013, vol. 1, pp. 651-679.
13 W. Gu and O. V. Ozerov, *Inorg. Chem.*, 2011, **50**, 2726-2728.
14 M. Wegener, F. Huber, C. Bolli, C. Jenne and S. F. Kirsch, *Chem. Eur. J.*, 2015, **21**, 1328-1336.
15 N. S. Hosmane, *Boron science: new technologies and applications*, Taylor & Francis Books/CRC, Boca Raton, 2012.
16 G. Crini, *Chem. Rev.*, 2014, **114**, 10940-10975.
17 J. Warneke, C. Jenne, J. Bernarding, V. A. Azov and M. Plaumann, *Chem. Commun.*, 2016, **52**, 6300-6303.
18 K. I. Assaf, M. S. Ural, F. Pan, T. Georgiev, S. Simova, K. Rissanen, D. Gabel and W. M. Nau, *Angew. Chem., Int. Ed.*, 2015, **54**, 6852-6856.
19 K. I. Assaf and W. M. Nau, *Angew. Chem., Int. Ed.*, 2018, **57**, 13968-13981.
20 K. I. Assaf, J. Holub, E. Bernhardt, J. M. Oliva-Enrich, M. I. Fernández Pérez, M. Canle, J. A. Santaballa, J. Fanfrlík, D. Hnyk and W. M. Nau, *ChemPhysChem*, 2020, **21**, 971-976.
21 S. M. Eyrilmez, E. Bernhardt, J. Z. Dávalos, M. Lepšík, P. Hobza, K. I. Assaf, W. M. Nau, J. Holub, J. M. Oliva-Enrich, J. Fanfrlík and D. Hnyk, *Phys. Chem. Chem. Phys.*, 2017, **19**, 11748-11752.
22 Z. Li, Y. Jiang, Q. Yuan, J. Warneke, Z. Hu, Y. Yang, H. Sun, Z. Sun and X.-B. Wang, *Phys. Chem. Chem. Phys.*, 2020, **22**, 7193-7200.
23 X.-B. Wang and L.-S. Wang, *Rev. Sci. Instrum.*, 2008, **79**, 073108.
24 W. H. Knoth, H. C. Miller, J. C. Sauer, J. H. Balthis, Y. T. Chia and E. L. Muetterties, *Inorg. Chem.*, 1964, **3**, 159-167.
25 V. Geis, K. Guttsche, C. Knapp, H. Scherer and R. Uzun, *Dalton Trans.*, 2009, 2687-2694.
26 D. V. Peryshkov, A. A. Popov and S. H. Strauss, *J. Am. Chem. Soc.*, 2009, **131**, 18393-18403.
27 T. Lu, *Molclus program*, Beijing Kein Research Center for Natural Science, Beijing, China, 2018, http://www.keinsci.com/research/molclus.html.
28 J. Řezáč and P. Hobza, *J. Chem. Theory Comput.*, 2012, **8**, 141-151.
29 J. J. P. Stewart, *J. Mol. Model.*, 2007, **13**, 1173-1213.
30 James J. P. Stewart *MOPAC2016*, Stewart Computational Chemistry, Colorado Springs, CO, USA, 2016.
31 Y. Zhao and D. G. Truhlar, *Theor. Chem. Acc.*, 2008, **120**, 215-241.
32 K. A. Peterson, D. Figgen, E. Goll, H. Stoll and M. Dolg, *J. Chem. Phys.*, 2003, **119**, 11113-11123.
33 F. Weigend and R. Ahlrichs, *Phys. Chem. Chem. Phys.*, 2005, **7**, 3297-3305.
34 S. Grimme, J. Antony, S. Ehrlich and H. Krieg, *J. Chem. Phys.*, 2010, **132**, 154104.
35 J. Zheng, X. Xu and D. G. Truhlar, *Theor. Chem. Acc.*, 2011, **128**, 295-305.
36 F. Weigend, M. Häser, H. Patzelt and R. Ahlrichs, *Chem. Phys. Lett.*, 1998, **294**, 143-152.
37 A. Schäfer, C. Huber and R. Ahlrichs, *J. Chem. Phys.*, 1994, **100**, 5829-5835.
38 K. Eichkorn, F. Weigend, O. Treutler and R. Ahlrichs, *Theor. Chem. Acc.*, 1997, **97**, 119-124.
39 A. Bergner, M. Dolg, W. Küchle, H. Stoll and H. Preuß, *Mol. Phys.*, 1993, **80**, 1431-1441.
40 L. Goerigk and S. Grimme, *Phys. Chem. Chem. Phys.*, 2011, **13**, 6670-6688.
41 S. F. Boys and F. d. Bernardi, *Mol. Phys.*, 1970, **19**, 553-566.
42 F. L. Hirshfeld, *Theor. Chim. Acta*, 1977, **44**, 129-138.
43 T. Lu and F. Chen, *J. Comput. Chem.*, 2012, **33**, 580-592.
44 B. Jeziorski, R. Moszynski and K. Szalewicz, *Chem. Rev.*, 1994, **94**, 1887-1930.

45 E. G. Hohenstein and C. D. Sherrill, *J. Chem. Phys.*, 2010, **132**, 184111.
46 E. G. Hohenstein, R. M. Parrish, C. D. Sherrill, J. M. Turney and H. F. Schaefer, *J. Chem. Phys.*, 2011, **135**, 174107.
47 T. M. Parker, L. A. Burns, R. M. Parrish, A. G. Ryno and C. D. Sherrill, *J. Chem. Phys.*, 2014, **140**, 094106.
48 E. Papajak, J. Zheng, X. Xu, H. R. Leverentz and D. G. Truhlar, *J. Chem. Theory Comput.*, 2011, **7**, 3027-3034.
49 E. Papajak and D. G. Truhlar, *J. Chem. Theory Comput.*, 2011, **7**, 10-18.
50 R. M. Parrish, L. A. Burns, D. G. A. Smith, A. C. Simmonett, A. E. DePrince, E. G. Hohenstein, U. Bozkaya, A. Y. Sokolov, R. Di Remigio, R. M. Richard, J. F. Gonthier, A. M. James, H. R. McAlexander, A. Kumar, M. Saitow, X. Wang, B. P. Pritchard, P. Verma, H. F. Schaefer, K. Patkowski, R. A. King, E. F. Valeev, F. A. Evangelista, J. M. Turney, T. D. Crawford and C. D. Sherrill, *J. Chem. Theory Comput.*, 2017, **13**, 3185-3197.
51 P. J. Stephens, F. J. Devlin, C. F. Chabalowski and M. J. Frisch, *J. Phys. Chem.*, 1994, **98**, 11623-11627.
52 G. te Velde, F. M. Bickelhaupt, E. J. Baerends, C. Fonseca Guerra, S. J. A. van Gisbergen, J. G. Snijders and T. Ziegler, *J. Comput. Chem.*, 2001, **22**, 931-967.
53 F. M. Bickelhauptm and E. J. Baerends, *Kohn-Sham Density Functional Theory: Predicting and Understanding Chemistry*, John Wiley & Sons, Inc, 2000, 1-86.
54 S. Grimme, S. Ehrlich and L. Goerigk, *J. Comput. Chem.*, 2011, **32**, 1456-1465.
55 E. R. Johnson, S. Keinan, P. Mori-Sanchez, J. Contreras-García, A. J. Cohen and W. Yang, *J. Am. Chem. Soc.*, 2010, **132**, 6498-6506.
56 C. Lefebvre, G. Rubez, H. Khartabil, J.-C. Boisson, J. Contreras-García and E. Hénon, *Phys. Chem. Chem. Phys.*, 2017, **19**, 17928-17936.
57 W. Humphrey, A. Dalke and K. Schulten, *J. Mol. Graph.*, 1996, **14**, 33-38.
58 M. J. Frisch, G. W. Trucks, H. B. Schlegel, G. E. Scuseria, M. A. Robb, J. R. Cheeseman, G. Scalmani, V. Barone, G. A. Petersson, H. Nakatsuji, X. Li, M. Caricato, A. V. Marenich, J. Bloino, B. G. Janesko, R. Gomperts, B. Mennucci, H. P. Hratchian, J. V. Ortiz, A. F. Izmaylov, J. L. Sonnenberg, Williams, F. Ding, F. Lipparini, F. Egidi, J. Goings, B. Peng, A. Petrone, T. Henderson, D. Ranasinghe, V. G. Zakrzewski, J. Gao, N. Rega, G. Zheng, W. Liang, M. Hada, M. Ehara, K. Toyota, R. Fukuda, J. Hasegawa, M. Ishida, T. Nakajima, Y. Honda, O. Kitao, H. Nakai, T. Vreven, K. Throssell, J. A. Montgomery Jr., J. E. Peralta, F. Ogliaro, M. J. Bearpark, J. J. Heyd, E. N. Brothers, K. N. Kudin, V. N. Staroverov, T. A. Keith, R. Kobayashi, J. Normand, K. Raghavachari, A. P. Rendell, J. C. Burant, S. S. Iyengar, J. Tomasi, M. Cossi, J. M. Millam, M. Klene, C. Adamo, R. Cammi, J. W. Ochterski, R. L. Martin, K. Morokuma, O. Farkas, J. B. Foresman and D. J. Fox *Gaussian 16 Rev. A.03*, Wallingford, CT, 2016.
59 R. F. W. Bader, *Chem. Rev.*, 1991, **91**, 893-928.
60 M. Mayer, V. van Lessen, M. Rohdenburg, G.-L. Hou, Z. Yang, R. M. Exner, E. Aprà, V. A. Azov, S. Grabowsky, S. S. Xantheas, K. R. Asmis, X.-B. Wang, C. Jenne and J. Warneke, *Proc. Natl. Acad. Sci.*, 2019, **116**, 8167.
61 M. J. Lecours, R. A. Marta, V. Steinmetz, N. Keddie, E. Fillion, D. O'Hagan, T. B. McMahon and W. S. Hopkins, *J. Phys. Chem. Lett.*, 2017, **8**, 109-113.
62 X.-B. Wang, *J. Phys. Chem. A*, 2017, **121**, 1389-1401.
63 L.-S. Wang and X.-B. Wang, *J. Phys. Chem. A*, 2000, **104**, 1978-1990.

64 M. K. Scheller, R. N. Compton and L. S. Cederbaum, *Science*, 1995, **270**, 1160.
65 X.-B. Wang, C.-F. Ding and L.-S. Wang, *Phys. Rev. Lett.*, 1998, **81**, 3351-3354.
66 X.-B. Wang and L.-S. Wang, *Annu. Rev. Phys. Chem.*, 2009, **60**, 105-126.
67 D. J. Tozer and N. C. Handy, *J. Chem. Phys.*, 1998, **109**, 10180-10189.
68 D. W. Arnold, S. E. Bradforth, E. H. Kim and D. M. Neumark, *J. Chem. Phys.*, 1995, **102**, 3493-3509.
69 H. Zhang, W. Cao, Q. Yuan, L. Wang, X. Zhou, S. Liu and X.-B. Wang, *Phys. Chem. Chem. Phys.*, 2020, **22**, 19459-19467.
70 S. Emamian, T. Lu, H. Kruse and H. Emamian, *J. Comput. Chem.*, 2019, **40**, 2868-2881.